



**HAL**  
open science

# Predictive Atomistic Model for Hydrogen Adsorption on Metal Surfaces: Comparison with Low-Energy Ion Beam Analysis on Tungsten

Zachary Piazza, Robert Kolasinski, Muthali Ajmalghan, Etienne Hodille, Yves Ferro

► **To cite this version:**

Zachary Piazza, Robert Kolasinski, Muthali Ajmalghan, Etienne Hodille, Yves Ferro. Predictive Atomistic Model for Hydrogen Adsorption on Metal Surfaces: Comparison with Low-Energy Ion Beam Analysis on Tungsten. *Journal of Physical Chemistry C*, 2021, 125 (29), pp.16086-16096. 10.1021/acs.jpcc.1c01068 . hal-03664140

**HAL Id: hal-03664140**

**<https://hal.science/hal-03664140v1>**

Submitted on 10 May 2022

**HAL** is a multi-disciplinary open access archive for the deposit and dissemination of scientific research documents, whether they are published or not. The documents may come from teaching and research institutions in France or abroad, or from public or private research centers.

L'archive ouverte pluridisciplinaire **HAL**, est destinée au dépôt et à la diffusion de documents scientifiques de niveau recherche, publiés ou non, émanant des établissements d'enseignement et de recherche français ou étrangers, des laboratoires publics ou privés.

# A Predictive Atomistic Model for Hydrogen Adsorption on Metal Surfaces: Comparison with Low Energy Ion Beam Analysis on Tungsten

Zachary A. Piazza<sup>a</sup>, Robert D. Kolasinski<sup>b</sup>, Muthali Ajmalghan<sup>a</sup>, Etienne A. Hodille<sup>a,†</sup>, and Yves Ferro<sup>a,\*</sup>

<sup>a</sup> *Laboratoire PIIM, Aix-Marseille Université/CNRS, Avenue escadrille Normandie-Niemen, 13397, Marseille, France*

<sup>b</sup> *Sandia National Laboratories, Plasma and Reacting Flow Science Department, Livermore, California 94 551, USA*

**ABSTRACT:** We present an analytical thermodynamic model of a surface in contact with a gas phase which enables us to determine the surface coverage of the adsorbate depending on the temperature, pressure and chemical potential of the gas. This model is applied to both the W(110) and W(100) surface of tungsten in contact with hydrogen. The thermodynamic model is built upon data computed by density functional theory that provide the complete electronic and vibrational energetics of both surfaces. It is further compared to experimental measurements of hydrogen coverage during isobar exposure at various temperature acquired via low energy ion scattering and direct recoil spectroscopy techniques. On W(110), the agreement is quantitative provided that an additional degree of freedom is added to the model. This degree of freedom accounts for the translational motion of the adsorbate along 1D channel on the surface. On W(100), surface reconstruction makes the energetics of the system more complex; the full details of the experimental isobar are not well reproduced, although the overall consistency is obtained. We end-up with a thermodynamic model based on DFT data having accurate predictive capabilities to determine the hydrogen coverage of tungsten at any  $p$  and  $T$ .

\* corresponding author: [yves.ferro@univ-amu.fr](mailto:yves.ferro@univ-amu.fr)

† current address: CEA, IRFM, F-13108 Saint Paul lez Durance, France.

## 1. INTRODUCTION

In this work, we have developed an analytical thermodynamic model built in the  $(\mu, p, T)$  ensemble that allows us to determine, based on density functional theory (DFT) data, the surface coverage of a metal in contact with a gas phase in case of strong chemisorption. The DFT data are herein computed for tungsten and hydrogen to which the model is applied. The model is subsequently benchmarked against experimental measurement of the hydrogen coverage during isobar adsorption at various temperatures from low energy ion scattering (LEIS) and direct recoil spectroscopy (DRS).

In some other approaches dealing with adsorption and based on 2D-Ising model<sup>1,2</sup> or transfer-matrix<sup>3,4</sup> methodologies, the adsorbate-adsorbate and adsorbate-substrate interactions are decomposed into pair and higher order effective clusters interactions according to a lattice gas models<sup>5,6</sup> in order to fit experimental results. Our approach follows a different methodology, and the interaction between the adsorbate and the substrate are computed by DFT with no parametrization against experimental results. Experiments however remain essential to validate the model, which is done for both the W(110) and W(100) surfaces.

As tungsten constitutes the divertor plates of JET<sup>7,8</sup>, WEST<sup>9</sup> and future ITER tokamaks<sup>10</sup>, a major application of this work is related to nuclear fusion sciences, plasma-material interactions, and the permeation of hydrogen isotopes into the first wall of tokamaks.

Experimentally, the processes that govern hydrogen retention in tungsten are typically investigated through thermal desorption spectroscopy (TDS) and permeation experiments. TDS data are typically analyzed with Macroscopic Rate Equations (MRE), which incorporate as much as possible a large variety of atomic-scale mechanisms, most of them being related to bulk properties. These mechanisms are characterized by physical quantities that are mostly established via density functional theory (DFT) calculations. Today, current MRE models

attempt to incorporate plausible surface mechanisms to improve their capability to reproduce as accurately as possible experimental TDS data<sup>11-16</sup>. However, what remains is the need to establish the coverage of the surface versus the experimental conditions to which it is exposed; this is precisely the aim of the present work.

Both the W(100) and W(110) surfaces are sampled into periodic minimal surface areas characterized by a discrete coverage  $\theta$ . The coverage  $\theta = \frac{n}{N}$  is defined as the number  $n$  of adsorbed atoms divided by the number  $N$  of substrate atoms on the top surface. The range of coverages investigated spans from the bare surface to over-saturation by steps of  $\Delta\theta = 0.25$ . For each coverage  $\theta$ , various configurations resulting from geometric optimization were considered. The probability of finding a minimal surface area at coverage  $\theta$  is then expressed as a function of the chemical potential of hydrogen  $\mu$ , the pressure  $p$ , and the temperature  $T$ . In the end, the macroscopic surface coverage  $\bar{\theta}(\mu, p, T)$  is given as the mean value of  $\theta$  over the whole surface.

The above results are compared with experimental measurements obtained using low energy ion scattering (LEIS) and direct recoil spectroscopy (DRS). In both cases, the composition information is obtained from classical scattering kinematics, whereas structural information can be extracted from surface channeling and shadowing effects. Since these measurements focus on measurements of surface composition, we emphasize these aspects of the technique here. Both LEIS and DRS are unique among surface analysis techniques for the sensitivity to chemisorbed hydrogen. Other commonly used surface composition techniques (primarily Auger electron spectroscopy and X-ray photoelectron spectroscopy) provide limited or no sensitivity to hydrogen, and other techniques such as thermal desorption spectroscopy often provide only indirect information. In the analysis presented below, we use DRS to detect and analyze the recoiled H and use this to make measurements of the surface coverage. LEIS, on the other hand, is used for detection of the W substrate.

The remainder of this paper is organized as follows: the details of the DFT calculations, of the thermodynamic model and of the experimental techniques are given in section 2. Section 3 provides the DFT data, the results of the thermodynamic model and of the experimental measurements. Section 4 organizes a general discussion about how the present model compares with the experimental data, and on the new insights it brings to the general understanding of the hydrogen to tungsten interaction. This is followed by section 5, where we provide some concluding remarks.

## 2. METHODOLOGY

### 2.1. Density Functional Theory surface model and numerical parameters

As in our previous studies of the interactions of hydrogen with tungsten surfaces<sup>17,18</sup>, herein we use a similar periodic plane-wave DFT model as implemented in Quantum Espresso package<sup>19</sup>. We employ the PBE exchange-correlation functional<sup>20</sup> and the Vanderbilt ultra-soft scalar-relativistic pseudo-potentials (USPP) to describe the ionic cores<sup>21</sup>; 14 valence and semi-core electrons were considered for tungsten. Energy cutoffs of 40 Ry and 320 Ry were used for the expansion of the wave-function and the electronic charge density, respectively. Vibrational frequencies of the hydrogen atoms were calculated via Density Functional Perturbation Theory<sup>22</sup> in the harmonic approximation. All other numerical parameters for electronic and vibrational calculations are identical to the ones described in Ref 17.

Both the W(110) and W(100) surfaces are modeled by a 6 layer slabs, keeping the bottom two layers of tungsten atoms frozen to bulk geometry, with a 20 Å vacuum inserted in the Z-direction. The dimension of the W(100) working-cell is  $2 \times 2 \times 6$  as in Ref 23 with the bulk *bcc* cell parameter  $\mathbf{a} = 3.187\text{\AA}$ . The surface working-cell, constructed upon  $2 \times 2$  repetition of the surface unit-cells, contains four tungsten atoms as shown in **Figure 1**. Correspondingly the

hydrogen coverage increases by steps of  $\Delta\theta = \frac{\Delta n}{N} = 0.25$ . The working-cell is periodically repeated in the three directions of space, making of the model a pseudo-2D periodic system.

Regarding the W(110) working cell, the *centered-rectangular*  $1 \times 1 \times 6$  working-cell initially used in Ref 23 was enlarged to a *rhombus* of double area of dimension  $a\sqrt{3} \times a\sqrt{3}$  also shown in **Figure 1**; it displays four tungsten atoms on the top surface too, allows for more hydrogen configurations to be investigated, and enables the coverage to vary by steps of  $\Delta\theta = 0.25$  as on the W(100) surface. For each coverage  $\theta$ , we computed all the lowest energy configurations  $j$  in a range of 0.2 eV.

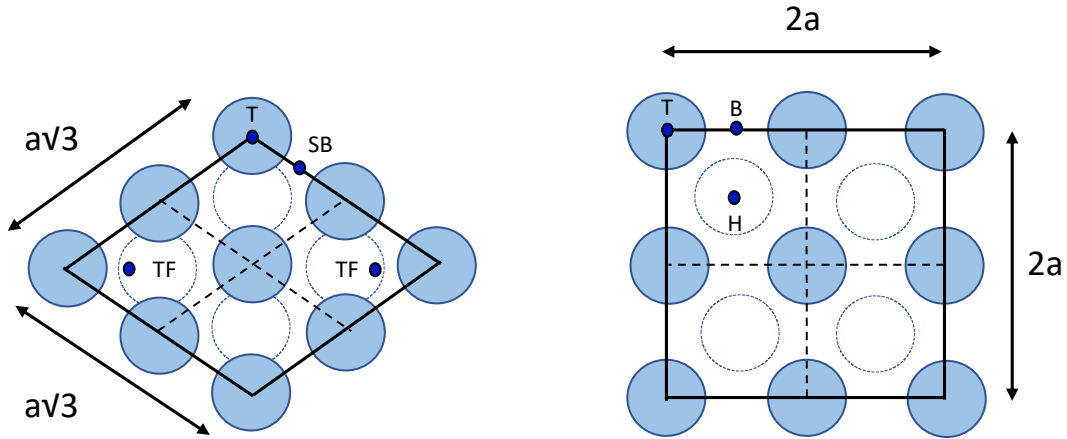


**Figure 1.** Schematic representation of the working-cell for the W(110) and W(100) surfaces. The top-surface W atoms are shown in blue, the W atom of the layer below are shown in light-blue. Adsorption sites are indicated by dark-blue dots: T (top), TF (three-fold), H(Hollow), B (bridge), SB (short-bridge). The W(100) is shown with no surface reconstruction. Upon reconstruction of the surface, B sites transforms into SB (short-bridge) sites and LB (long-bridge) sites as can be seen in the Supplementary Information. The 1D diffusion paths for hydrogen on both the W(100) and W(110) surfaces are shown with brown dotted lines

The adsorption energies are calculated as follows:

$$E_{ad,H_n} = E_{W_{slab},H_n}^{DFT} - E_{W_{slab}}^{DFT} - \frac{n}{2} E_{H_2}^{DFT} \quad (1)$$

where  $n$  is the number of hydrogen atoms,  $E_{W_{slab},H_n}^{DFT}$  is the energy value of a given configuration of  $n$  hydrogen atoms on a tungsten surface,  $E_{W_{slab}}^{DFT}$  is the energy of the corresponding bare

surface, and  $E_{H_2}^{DFT}$  is the calculated value of molecular  $H_2$ . We also provide zero-point vibrational energy (ZPE) corrected values for all adsorption energies, labeled as  $E_{ad,ZPE,H_n}$ . As the coverage ratio is increased, the change in adsorption energy of the most stable configurations is calculated as:

$$E_{ad}^{n+1} = E_{W_{slab,H_{n+1}}}^{DFT} - E_{W_{slab,H_n}}^{DFT} - \frac{1}{2}E_{H_2}^{DFT} \quad (2)$$

## 2.2. Thermodynamic model of the surface

First, we need to define the system; it is the surface of tungsten either in the (110) or (100) orientation. The system is open and can accommodate a varying number of hydrogen atoms. It is in equilibrium with a large enough hydrogen reservoir and a thermostat so that adsorption and desorption of hydrogen leaves the pressure and temperature unaffected. Consequently, the external parameters that control the system are the pressure, temperature and chemical potential of hydrogen.

The grand-partition function of the system  $\tilde{\Xi}(p, T, \mu)$  is built upon all of the configurations and associated energetics established by DFT. The variation in volume of the surface is considered negligible after adsorption or desorption of hydrogen, making the volume to remain constant at  $V_0$ . As hydrogen is supposed to be strongly bonded to the surface, only the electronic and vibrational energies are considered in a first step for building  $\tilde{\Xi}(p, T, \mu)$ . As a consequence, the range of validity of the model is the harmonic approximation for computing the vibrational frequencies, leading us to consider temperature below approximately 1000K. In the following of the sub-section and for the sake of simplicity, the energy  $E_{W_{slab,H_n}}^{DFT}$  computed for a working-cell at coverage  $\theta = \frac{n}{4}$  in configuration  $j$  will simply be referred as  $E_j^\theta$ . In the same way, the sum over all of the vibrational modes of configuration  $j$ , and over all levels of each vibrational mode  $j$  will be simply written as  $\sum_{vib} E_{j,vib}^\theta$ .

Using these notations, the grand-partition function expresses as:

$$\tilde{\Xi}(p, T, \mu) = \sum_{\theta} \left( \sum_{j \rightarrow \theta} \sum_{vib,j} \gamma_j \exp [-\beta(E_j^{\theta} + E_{j,vib}^{\theta} + pV_o)] \right) \exp(\beta n_{\theta} \mu) \quad (4)$$

where  $\beta$  is  $1/k_B T$  and  $\gamma_j$  is the number of symmetrically equivalent configurations  $j$  at coverage  $\theta$ .

In practice, it would suffice to consider only the most probable configuration or the configurations that coexist at a given coverage  $\theta$ . However, the adsorption energy depends on the temperature through the vibrational frequencies which itself depends of the geometry of adsorption. Consequently, it is not obvious how to determine at a given temperature which is the most stable configuration or which are the degenerated ones. We consequently consider all of the configurations and will further illustrate in Figure 4 which are the ones of significant weigh in the partition function.

Equation (4) contains  $\tilde{\mathcal{Z}}_j^{\theta}(n_{\theta}, p, T) = \sum_{vib,j} \exp [-\beta(E_j^{\theta} + E_{j,vib}^{\theta} + pV_o)]$ . Since  $g_j^{\theta} = -kT \ln \tilde{\mathcal{Z}}_j^{\theta}$ , where  $g_j^{\theta}$  is the Gibbs-free energy of configuration  $j$  at coverage  $\theta$ , the grand partitions function simplifies to:

$$\tilde{\Xi}(p, T, \mu) = \sum_{\theta} \sum_{j \rightarrow \theta} \gamma_j \exp [-\beta(g_j^{\theta} - n_{\theta} \mu)] \quad (5)$$

The Gibbs free energy  $g_j^{\theta}(p, T, n_{\theta})$  is calculated as  $g_j^{\theta} = (E_j^{\theta} + h_{vib}) - T s_{vib}$  where  $h_{vib}$  and  $s_{vib}$  are given in [Appendix](#).

Regarding the chemical potential  $\mu$  of hydrogen in the reservoir, it is simply calculated as  $\mu(p, T) = \frac{1}{2} g_{H_2}(p, T)$ . (Also see the [Appendix](#) for further details.) As the range of pressure here considered is from below atmospheric pressure down to ultra-high vacuum, hydrogen is assumed to behave like an ideal gas, leading to  $\mu(T, p) = \mu^{\circ}(T) + RT \ln \left( \frac{p_{H_2}}{p^{\circ}} \right)$  where  $p^{\circ}$  and



$\mu^\circ$  are the standard pressure of 1 bar and the chemical potential of hydrogen at standard pressure.

As a result, the temperature and the partial pressure of hydrogen  $p_{H_2}$  determine the chemical potential and consequently the whole properties of the system at equilibrium.

The probability of finding a unit-cell at coverage  $\theta$  in configuration  $j$  is:

$$P_{\theta_j} = \frac{\gamma_j \exp[-\beta(g_j^\theta - n_\theta \mu)]}{\tilde{\Xi}(p, T, \mu)} \quad (6)$$

The probability of finding a working-cell at coverage  $\theta$  regardless of the configuration is:

$$P_\theta = \frac{\sum_{j \rightarrow \theta} \gamma_j \exp[-\beta(g_j^\theta - n_\theta \mu)]}{\tilde{\Xi}(p, T, \mu)} \quad (7)$$

The macroscopic coverage  $\bar{\theta}$  in hydrogen of the whole surface is the sum of the probability  $P_\theta$  of having coverage  $\theta$  on a given working-cell:

$$\bar{\theta} = \sum_{\theta=0}^{\theta_{max}} \theta \cdot P_\theta \quad (8)$$

In the end, the macroscopic coverage  $\bar{\theta}$  is a continuous function of temperature and pressure, despite it being based on discrete atomic-scale coverages and configurations  $\theta_j$  computed by DFT, but fully reflects the real case seen at the atomic scale. Given the quasi-harmonic approximations made for the vibrations of the adsorbate and the assumed ideal behavior of the gas phase, the range of validity of the model for temperature and pressure is below approximately 1000 K and 1 bar, respectively.

### 2.3. LEIS and DRS measurements

As in our previous work<sup>23</sup>, we used an angle resolved ion energy spectrometer (ARIES) for surface characterization. A W single crystal (MaTecK GmbH) was aligned and polished to within 0.1° of the (110) plane. The specimen was attached to a button-style heater using Ta

wire, allowing it to be annealed to 500 °C. Our manipulator allows for both polar and azimuthal rotation of the sample. For surface cleaning, we initially sputter-cleaned the sample at grazing incidence during continuous azimuthal rotation using a Ne<sup>+</sup> ion beam. The sample was also annealed at 500 °C in between cleaning cycles, as we monitored the LEIS spectra for any chemisorbed impurities. Once the cleaning process was completed, a mass-separated 2 keV Ne<sup>+</sup> was then used to probe the surface during the LEIS/DRS measurements, and the scattered and recoiled particles were characterized using a hemispherical electrostatic analyzer. While the vacuum within our system is generally quite good ( $< 5 \times 10^{-10}$  Torr), the chief impurity within our system is hydrogen. As a result, there is at least some residual hydrogen that can be detected on the W surface even when it was not being dosed with any gases, and this can add an increased background to our measurements. For this reason, we dosed our surfaces with D<sub>2</sub> gas at varying partial pressures to distinguish from the background H.

### 3. RESULTS

#### 3.1 – Density Functional Theory data for hydrogen adsorption at various coverages and configurations.

The energetics of all of the coverages and configurations we computed by DFT for hydrogen on top of tungsten are graphically displayed in **Figure 2** and **Figure 3** and summarized in **Table 1** and **Table 2** for the W(110) and W(100) surface, respectively. In each Table are displayed the various coverages we computed, the low energy configurations  $j$  we determined after geometry optimizations, the degeneracy  $\gamma_j$  of each configuration resulting from symmetry equivalent positions, the adsorption energy  $E_{ad,H_n}$  calculated using eq. (1), and the adsorption energy of adding an additional hydrogen atom  $E_{ad}^{n+1}$  calculated according to eq(2).

**Table 1.**

Hydrogen adsorption on the W(110) surface: the adsorption energies  $E_{ad,H_n}$  and the adsorption energy of adding an additional atom  $E_{ad}^{n+1}$  are given with ZPE correction for all the coverages  $\theta$  and configuration  $j$ . The number  $\gamma_j$  of symmetry equivalent positions for a given configuration  $j$  is also provided.  $E_{ad,H_n}$  is in eV *per*  $n$  hydrogen atoms,  $E_{ad}^{n+1}$  is eV *per* H atom.

$\theta$	$j$	$\gamma_j$	$E_{ad,H_n}$	$E_{ad,ZPE}$	$E_{ad,ZPE}^{n+1}$
0.25	1	8	-0.73	-0.68	-0.68
	2	8	-0.62	-0.58	
0.50	1	4	-1.47	-1.38	-0.70
	2	4	-1.47	-1.38	
	3	4	-1.43	-1.35	
	4	8	-1.35	-1.25	
	5	4	-1.30	-1.22	
0.75	1	8	-2.17	-2.03	-0.65
	2	2	-1.90	-1.75	
1.00	1	2	-2.80	-2.63	-0.60
	2	2	-2.47	-2.27	
1.25	1	2	-2.89	-2.62	+0.01
	2	2	-2.86	-2.59	
1.50	1	2	-3.03	-2.69	-0.07
	2	2	-2.97	-2.65	
	3	2	-2.91	-2.59	
1.75	1	1	-2.85	-2.44	+0.25
	2	1	-2.74	-2.35	
2.00	1	1	-2.68	-2.19	+0.25
	2	1	-2.41	-1.92	
	3	1	-2.35	-1.83	

**Table 2.**

Hydrogen adsorption on the W(100) surface: the adsorption energies  $E_{ad,H_n}$  and the adsorption energy of adding an additional atom  $E_{ad}^{n+1}$  are given with ZPE correction for all the coverages  $\theta$  and configurations  $j$ . The number  $\gamma_j$  of symmetry equivalent positions for a given configuration  $j$  is also provided.  $E_{ad,H_n}$  is in eV *per n* hydrogen atoms,  $E_{ad}^{n+1}$  are in eV *per H* atom.

$\theta$	$j$	$\gamma_j$	$E_{ad}$	$E_{ad,ZPE}$	$E_{ad,ZPE}^{n+1}$
0.25	1	6	-0.88	-0.83	-0.83
0.50	1	2	-1.79	-1.69	-0.86
	2	6	-1.63	-1.54	
0.75	1	2	-2.38	-2.22	-0.53
	2	4	-2.16	-2.02	
1.00	1	4	-3.10	-2.86	-0.64
	2	1	-3.02	-2.79	
	3	2	-2.99	-2.78	
	4	2	-2.89	-2.72	
1.25	1	4	-3.85	-3.58	-0.72
	2	4	-3.72	-3.45	
	3	4	-3.68	-3.44	
1.50	1	4	-4.51	-4.19	-0.61
	2	2	-4.44	-4.11	
1.75	1	2	-5.24	-4.84	-0.65
2.00	1	1	-5.98	-5.49	-0.65
2.25	1	4	-6.00	-5.48	+0.01
	2	1	-5.86	-5.30	
2.50	1	4	-5.94	-5.39	+0.09
	2	8	-5.96	-5.37	
	3	2	-5.91	-5.35	
	4	8	-5.94	-5.38	
2.75	1	4	-5.96	-5.31	+0.08
	2	8	-5.93	-5.24	
	3	4	-5.91	-5.28	
	4	8	-5.90	-5.25	
	5	4	-5.89	-5.27	
3.00	1	8	-5.95	-5.22	+0.09
	2	2	-5.89	-5.16	
	3	8	-5.84	-5.13	
	4	1	-5.82	-5.05	
3.25	1		-5.49	-4.76	+0.46

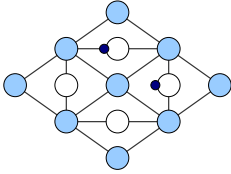
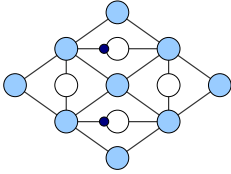
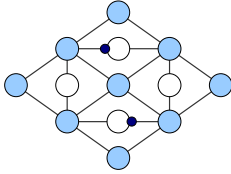
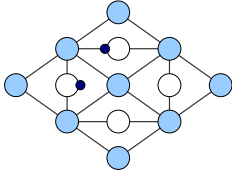
### 3.1.1. The W(110) surface

Regarding the W(110) surface, additional coverages and configurations (shown in the **SI**) were computed as compared to Ref 23. The three-fold (TF) position is known to be the most stable adsorption site on the W(110) surface<sup>24</sup>. Due to the size of the working-cell, only one

configuration was accessible at  $\theta = 0.50$  in Ref 23. In the present work, four TF-based adsorption configurations ( $j = 1-3$  and 5) were found (**Table 3** and **SI**); the two most stable ones are degenerate at  $E_{ad,ZPE} = 1.38$  eV and represent adsorption of hydrogen atoms parallel to the [110] and [100] directions. It is worth noting that configuration  $j = 1$  of coverages  $\theta = 0.50, 0.75$  and  $\theta = 1.00$  (given in **SI**) were experimentally observed at  $T = 110$ K by LEED<sup>25,26</sup> and correspond to the  $p(2 \times 1)$ ,  $p(2 \times 2)$  and  $p(1 \times 1)$  phases. Above 200K-250K, these phases become disorganized due to the mobility of the adsorbate.

**Table 3.**

Top-down schematic representations with corresponding adsorption energies  $E_{ad,ZPE}$  and hydrogen adsorption energies for  $\theta = 0.50$  three-fold configurations on the W(110) surface. Light blue circles represent tungsten surface atoms, white circles represent the layer beneath. Adsorbed hydrogens are represented in dark blue. Adsorption energies are in units of eV.

	tf1	tf2	tf3	tf4
				
$E_{ad,H_n,ZPE}$	-1.38	-1.38	-1.35	-1.22

The full energy diagram of all configurations in **Figure 2** shows a nearly linear decrease in  $E_{ad,H_n,ZPE}$  from the bare surface up to coverage 1.0, with a slope of  $-0.68$  eV/ $H_{atom}$  ( $\theta \leq 1.0$ ); this indicates weak interactions between neighboring ad-atoms. Above coverage 1.0, the *per* hydrogen adsorption energy  $E_{ad}^{n+1}$  increases drastically. However, the overall adsorption energy is at a minimum when  $\theta = 1.50$ . This is in contrast to our previous study<sup>23</sup> where the minimum was found at  $\theta = 1.00$  as a consequence of using a too small *centered-rectangular* (1×1) unit cell. This new result suggests  $\theta = 1.50$  could be the saturation limit at near 0 K, despite  $E_{ad,H_n}$  vs.  $\theta$  remains flat in the  $\theta = 1.0 - 1.5$  region. At  $\theta = 1.75$ , both the adsorption energy *per* hydrogen and the overall adsorption energy are increasing, thus coverages of  $\theta \geq 1.75$  are

unlikely to be physically relevant. Indeed, we previously computed<sup>23</sup> that coverage  $\theta = 2.00$  cannot be exceeded since  $\text{H}_2$  spontaneously recombines above this level. Moreover, the probability of having coverage beyond  $\theta = 1.50$  is herein zero in the condition of temperature and pressure belonging to the range of validity of the model.

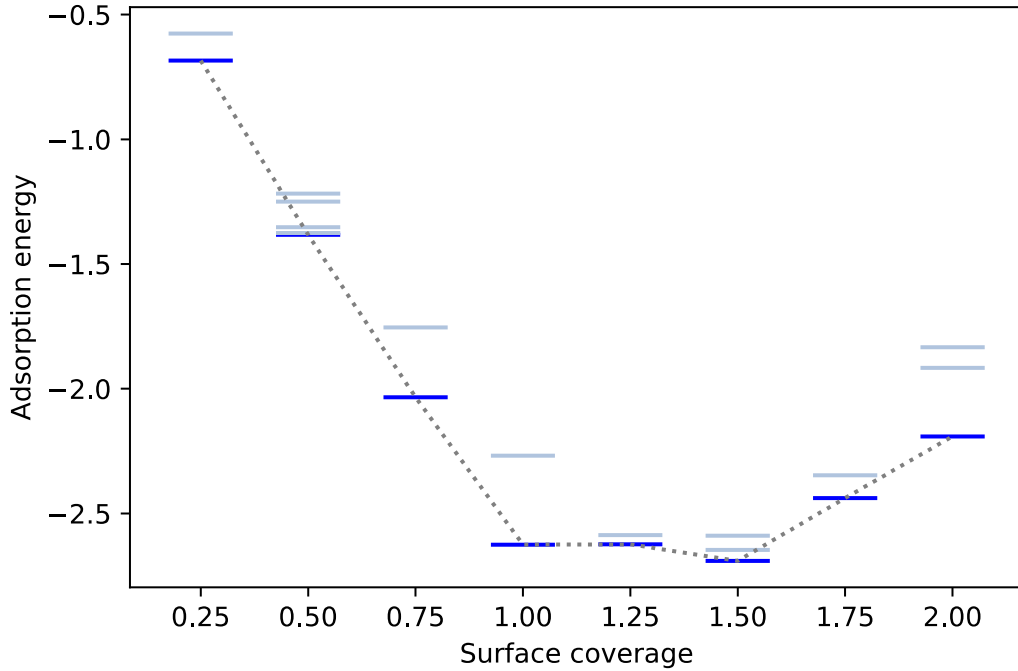


**Figure 2.** Energy trends of hydrogen adsorbed on the W(110) surface *versus* coverage ratio ( $\theta$ ). The adsorption energy  $E_{ad,H_n}$  given in eV *per n* hydrogen atoms is ZPE corrected. The most stable configuration is shown in dark blue for each computed coverage. Other configurations are displayed in light-blue.

### 3.1.2. The W(100) surface

Regarding the W(100) surface, additional configurations were also computed as compared to Ref 23. More combinations of short-bridges (SB) positions were added to the model between coverage  $\theta = 1.00$  and  $\theta = 2.00$ , sometimes resulting in lowering  $E_{ad,H_n,ZPE}$  by few tenths of eV. Some additional configurations were also built beyond coverage  $\theta = 2.00$  with mixing SB, TF and top (T) positions (all of them displayed in the **SI**). The full energy diagram shown in **Figure 3** however displays the same trend of adsorption energy  $E_{ad,H_n,ZPE}$  versus the coverage  $\theta$  as in Ref 23: at low coverage, the *per* hydrogen atom adsorption energy  $E_{ad,ZPE}^{n+1}$

is around  $-0.8\text{eV}$  as the results of the well-known surface reconstruction<sup>27-30,23</sup>. Then the trend is similar to the one of the W(110) surface with  $E_{ad}^{n+1}$  around  $-0.65\text{eV}$  up to coverage  $\theta = 2.00$ , which is the minimum of the curve. Above  $\theta = 2.00$ ,  $E_{ad}^{n+1}$  increases slowly, then sharply above  $\theta = 3.00$ , making higher coverages physically irrelevant. As previously mentioned, higher coverages were computed in Ref. 23 and spontaneously led to  $\text{H}_2$  recombination above  $\theta = 4.00$ . Additionally, the probability of finding coverages above  $\theta = 2.00$  is zero within the conditions of pressure and temperature that belong to the range of validity of the present model.

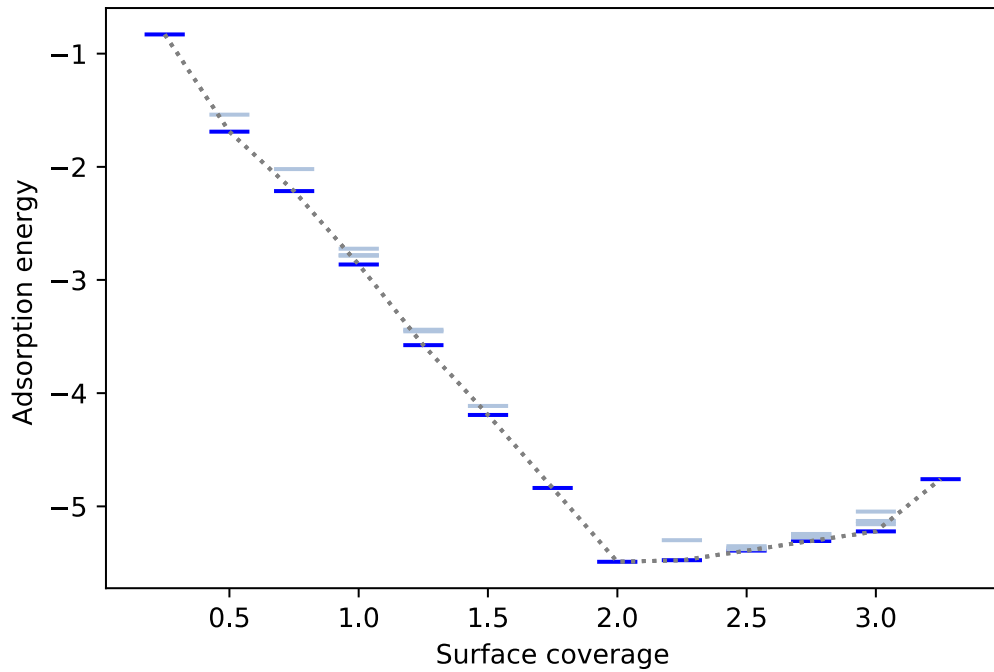


**Figure 3.** Energy trends of hydrogen adsorbed on the W(100) surface *versus* coverage ratio ( $\theta$ ). The adsorption energy  $E_{ad,H_n}$  given in eV *per n* hydrogen atoms is ZPE corrected. The most stable configuration is shown in dark blue for each computed coverage. Other configurations are displayed in light-blue.

### 3.2 – Building a thermodynamic model upon DFT data

The grand partition function of the system is built for both the W(110) and W(100) surfaces.

To this end, the Gibbs free energy  $g_j^\theta$  function of equation (5) is calculated for all configuration  $j$  at coverage  $\theta$  based on the electronic energies and vibrational frequencies computed by DFT

as presented above. The configurational entropy is considered through the degeneracy coefficient  $\gamma_j$  given in eq (5-7) and listed in **Table 1 and 2**.

**Figure 4** displays on the W(110) an example of what the model provides: the macroscopic coverage  $\bar{\theta}$  is plotted in bold black line at a pressure of  $10^{-8}$  torr versus temperature. Since the only gas in the reservoir is hydrogen, the total pressure is the partial pressure of hydrogen, which consequently determines its chemical potential through  $\mu(T, p) = \mu^\circ(T) + RT \ln\left(\frac{p_{H_2}}{p^\circ}\right)$ .

Up to  $T = 300$  K, the surface is saturated ( $\theta = 1$ ). As the temperature increases, the coverage decreases to  $\theta = 0$  by  $T = 600$ K. **Figure 4** also provides the probabilities  $P_{\theta_j}$  of equation (7) of finding locally configuration  $j$  at coverage  $\theta$  on the surface. The plot is limited to two configurations  $j = 1$  and 2 (bold and dotted lines) for the sake of readability.

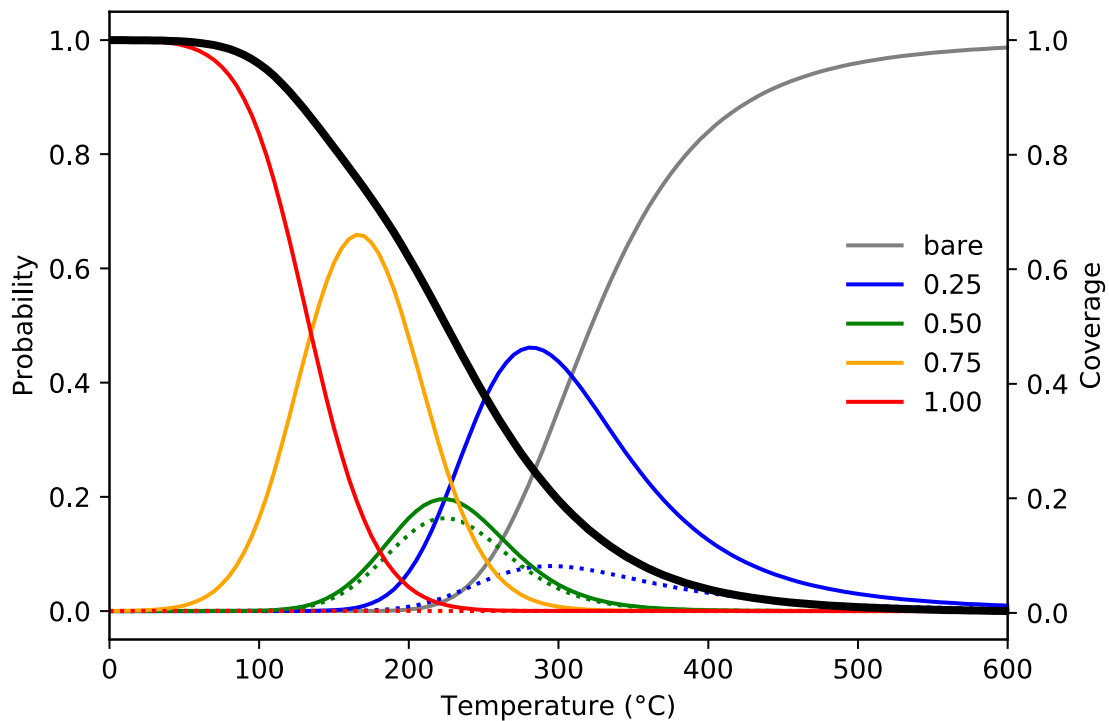


**Figure 4.** Coverage in hydrogen of the W(110) surface versus coverage the temperature in °C plotted in black bold line for a pressure of  $10^{-8}$  torr. The probability of finding the most relevant configurations is also plotted for coverages  $\theta = 0.25, 0.50, 0.75$  and  $1.00$ . For each coverage, the bold line represents the first configuration with the lowest adsorption energy and highest probability, dotted line displays the second configuration.



In order to check that we considered a complete set of configurations to build the model with no near-degenerate configuration left behind, we calculated a mean coverage  $\bar{\theta}'$  in the same way as  $\bar{\theta}$ , while removing the highest energy configuration at each coverage. As a result, the relative error  $\frac{|\bar{\theta}' - \bar{\theta}|}{\bar{\theta}}$  does not exceed 1% at coverage  $\theta = 0.2$  and 3% at coverage  $\theta = 0.1$ . (The mean error is expected to be maximum at low coverage and high temperature). This confirms that we considered enough configurations to have a well-converged model in this work.

### 3.2. LEIS and DRS measurements

In **Figure 5(a)** we show ion energy spectra that illustrate how the detected flux of recoiled hydrogen, which is to a reasonable approximation proportional to surface coverage, diminishes in intensity with increasing temperature. Here we use the notation D(R) to refer to H recoiled from the surface by the incident  $\text{Ne}^+$  beam. A range of temperatures is shown between 47 – 400 °C. Note that in this plot, an offset of 1000 counts/nC is added to each curve so that the peak shape is visible at different temperatures. The primary recoil peak is located at a relative energy of  $E/E_0 = 0.16$ , where  $E_0$  is the primary beam energy (2 keV). Additional higher energy peaks present due to multiple in-plane collisions between the recoiled H and the adjacent W atoms. The data shown in **Figure 5(b)** corresponds to the signal produced by  $\text{Ne}^+$  ions scattering from the W substrate (labelled here as W(QS), where QS indicates “quasi-single” collisions.) The variation in the W(QS) peak height with temperature is much more modest. The presence of the chemisorbed H layer only slightly shields the W substrate from the 2 keV  $\text{Ne}^+$  beam used to probe the surface.

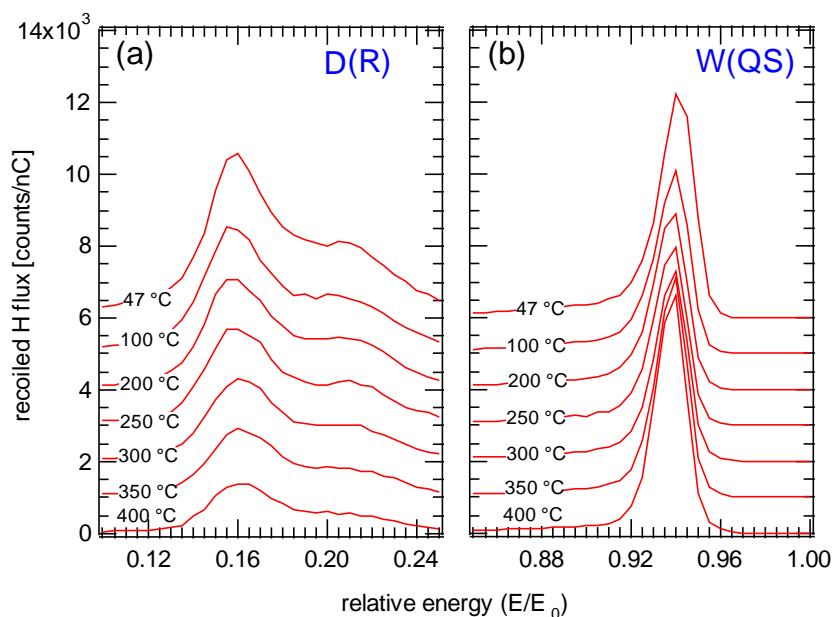


**Figure 5.** Ion energy spectra showing peaks due to (a) recoiled D chemisorbed on the surface and (b) scattering from the W(110) substrate. These measurements were taken while dosing the surface with molecular  $D_2(g)$  at a partial pressure of  $3 \times 10^{-7}$  Torr.

To examine how the surface coverage varies in real time during heating and cooling of the specimens, we monitored the height of the D(R) and W(QS) curves while dosing the surface with different partial pressures of  $D_2$ . The resulting curves are shown in **Figure 6**. To account for differences in ion beam current between each run, the data are normalized by taking the ratio of the D(R) and W(QS) peak heights. In each case, the sample was heated at a rate of  $15.8$   $^{\circ}C/min.$  up to a temperature of  $450$   $^{\circ}C$ . The temperature was held at this value for  $5$  min., and then cooled at the same rate down to room temperature ( $25$   $^{\circ}C$ ). We explored the effect of a range of heating rates, found that rates slower than  $15.8$   $^{\circ}C/min.$  had a negligible effect on the adsorption/desorption process. Because the heating process resulted in the desorption of chemisorbed impurities as well as D, re-adsorption of hydrogen during cooling was found to be a more reproducible indicator of the D concentration as a function of temperature. Three different partial pressures were examined, as indicated in **Figure 6**.

### 3.3. Results of the model

The coverage versus temperature curves for both the W(110) and W(100) surfaces are plotted in **Figure 6** for three different values of the pressure in hydrogen corresponding to the pressure used in experiment.

Interestingly, for the W(110) surface a coverage  $\theta = 1.50$  is never reached and saturation is obtained at coverage  $\theta = 1.00$ . This is in correspondence with experimental observations<sup>31</sup>, and is easily understood by the fact that such a coverage is disfavored by entropic effect - the entropy of the gas phase is larger than that of the adsorbate. Additionally, **Figure 6** shows that the coverage decreases smoothly from saturation to the bare W(110) surface as the temperature increases.

On the W(100) surface, saturation corresponds to  $\theta = 2.00$ , which also corresponds to experimental observation<sup>31</sup>. However, a sharp drop from  $\theta = 2.00$  to  $\theta = 0.50$  is obtained as a result of the surface reconstruction, which is strong from  $\theta = 0.00$  up to  $\theta = 0.50$ , and results in a stronger adsorption of hydrogen on the surface as shown by DFT<sup>23</sup>. This surface reconstruction was experimentally shown to vanish above 380 K<sup>27</sup>, while most of the desorption process takes place above this temperature. Since the DFT model can only account for zero temperature geometries and related vibrational frequencies, the low-coverage geometries and energetics in the model consequently differ from the high-temperature geometries of the adsorbate in the condition of the experiment.

As a result, the above considerations make the W(110) surface a real test-case for the model with regard to the adsorption of hydrogen. On the other hand, the W(100) + H system adds an additional level of complexity with the reconstruction of the surface that is lifted whilst desorption occurs, which is not considered in the present model.

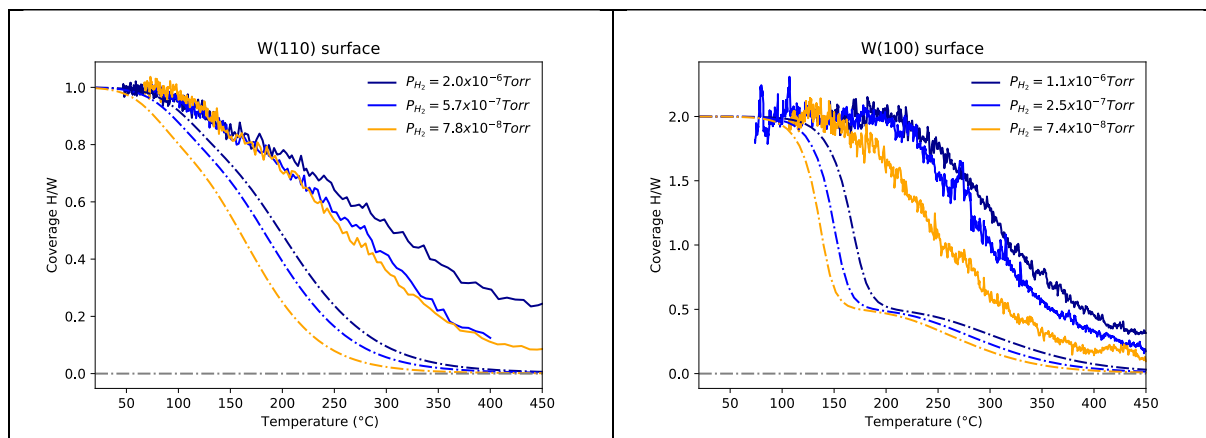


**Figure 6.** Absorption isobars while dosing with molecular  $D_2$  at varying pressures: left on the W(110) at  $p = 2.0 \times 10^{-6}$ ,  $5.7 \times 10^{-7}$  and  $7.8 \times 10^{-8}$  Torr, right on W(100) at  $p = 1.1 \times 10^{-6}$ ,  $2.5 \times 10^{-7}$  and  $7.4 \times 10^{-8}$  Torr. Here, the data is shown in terms of the ratio of the D(R) peak height to the W(QS) peak height and normalized to  $\theta = 1.00$  for on W(110) and 2 on W(100) at saturation. In dashed line are also plotted the coverages calculated with the thermodynamic model based on DFT for the three same values of the pressure as in the experiment.

## 4. DISCUSSION

### 4.1. Thermodynamic model versus LEIS and DRS results

#### 4.1.1 – W(110) surface

In **Figure 6**, both experimental and theoretical results are qualitatively consistent: lower pressure implies lower temperature for desorption, and the trend and shape of the  $\theta$  versus  $T$  curve are well reproduced. From a quantitative point of view, the temperature at which hydrogen start to desorb matches well between both the experiment and the model. Above this point, the disagreement becomes larger as the temperature increases. This is consistent with an entropic effect, and could be due to the motion of the adsorbate that increases with increasing temperature. In this case, hydrogen would diffuse on the surface, leading to an additional degree of freedom (namely the translation), which the current model does not consider.

In the literature, the difficulty in modelling the entropy of an adsorbate was recently pointed out<sup>32,33</sup>, as the adsorbate would retain part of the entropy it has in the gas phase when adsorbed on the surface. More specifically for tungsten, Balden et al.<sup>26</sup> and Gonchar et al.<sup>25</sup> showed the

organization of the substrate is lost at a temperature exceeding 200K, indicating hydrogen moves on W(110) above this temperature. Interestingly Bladen et al.<sup>34</sup> attempted to explain an anomaly in the surface phonon dispersion for the hydrogen covered W(110) surface by the propensity of the adsorbate to freely move in one direction. This 1D translation is confirmed by recent DFT calculations that established an activation barriers as low as 0.07 eV for hydrogen along a 1D channel of the W(110) surface. More precisely, Bergstrom et al.,<sup>35</sup> and Nojima et al.<sup>24</sup> established two diffusion paths for hydrogen on the W(110) plane: one along the TF-LB-TF adsorptions sites with related activation barrier of 0.30 eV, and another one along the TF-SB-TF path with an activation barrier of 0.07 eV. In the  $z$ -direction, the activation barrier for desorption is much higher at around 0.8eV<sup>17</sup>. As a result, the propensity of hydrogen to move almost freely in 1D only along the TF-SB-TF path of W(110) would be established. Of course, at very low temperature, a barrier of 70 meV would become significant. But at the same time, tunneling effects would become significant too. This point is nevertheless out of the scope of the present work, since below room temperature, the surface is already saturated. Additionally, most of the experimental results for validation are acquired above the temperature (120K to RT) at which tunneling is expected to happen.

We consequently added the translation Gibbs free energy  $g_{trans, n_H}$  of a 1D gas made of  $n$  indistinguishable hydrogen atom in the Boltzmann approximation along the TF-SB-TF channel to the total Gibbs free energy of the system.

$$g_{trans, n_H} = - n_H k_B T \left[ 1 + \ln \left( \sqrt{\frac{2\pi m k_B T}{h}} \frac{a_{path}}{n_H} \right) \right] \quad (9)$$

In eq (9),  $m$  is the mass of a hydrogen atom,  $h$  and  $k_B$  Planck's and Boltzmann's constants, and  $a_{path}$  is the total length of the path in the working-cell. The path is shown in dotted brown line in Figure 1, its length is  $a_{path} = 4 \mathbf{a}_{bulk}$ .

The resulting coverage *versus* T plot is shown in **Figure 7**. The comparison is much improved between both experimental and theoretical plots at each experimental pressure investigated, leading to a quantitative agreement.

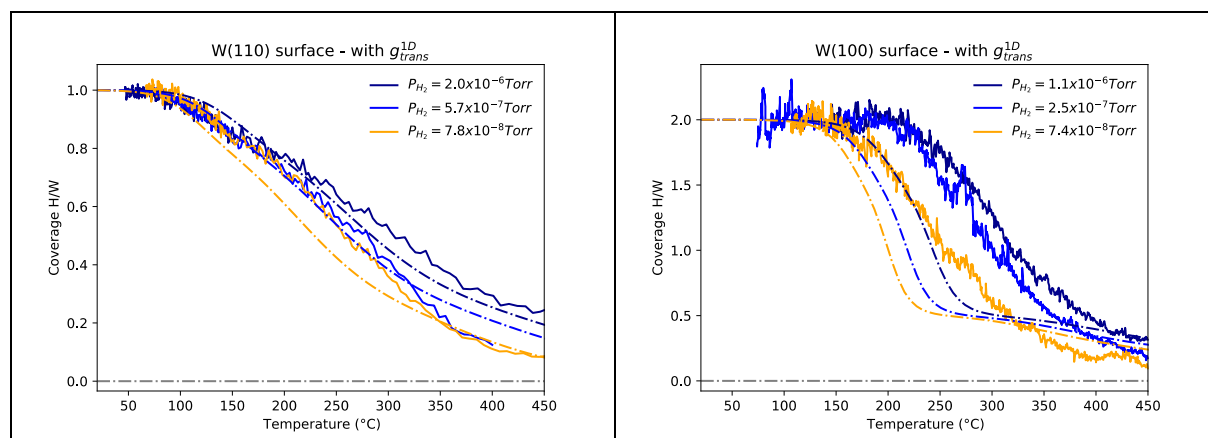


**Figure 7.** same as Figure 6 but with adding the translation Gibbs free-energy of a 1D gas to the Thermodynamic model.

#### 4.1.2 –W(100) surface

The reconstruction of the W(100) surface makes its energetics more complex to determine as compared with the W(110) surface. Bergstrom et al.<sup>35</sup> however established by DFT two activation barriers for the diffusion of hydrogen on the bare W(100) surface; they are 0.44 eV and 0.67 eV along SB-SB and SB-LB-SB paths, respectively on the reconstructed surface. However, the reconstruction is lost at the temperature of the experiment where hydrogen desorbs, and there is no reconstruction anymore at coverage  $\theta = 1.00$  and above. This could have a significant impact, potentially reducing the height of the barriers for the diffusion of hydrogen. As a result, hydrogen could diffuse along a 1D path leading from bridge-to-bridge sites.

Despite the uncertainty that exists on the diffusion and adsorption energy of hydrogen at elevated temperature, we nevertheless added the same translation Gibbs free energy of equation

(9) to the Gibbs free energy of the system as on the W(110) surface. Following a bridge-to-bridge diffusion path shown in brown dotted lines in **Figure 1**, we set  $a_{path}$  to  $8\sqrt{2} a_{bulk}$ . The result is plotted in **Figure 7**. While the model fails to reproduce the full details of the experimental isobars, probably as a consequence of the complexities introduced by surface reconstruction, the translational Gibb's free energy of hydrogen along 1D channels significantly improves the comparison with experimental results. The physics mechanisms underlying how this additional term improves the fit requires further investigation, though a reasonable explanation may be that it helps approximate the additional degree of freedom for the chemisorbed hydrogen enabled by the increase in the temperatures.

Additional experimental factors may also influence the comparison between the experiments and models. For example, we assume that the coverage is directly proportional to the peak height in the ion energy spectrum. Because the electrostatic analyzer used in the measurements only detects charged species, changes in neutralization may affect the measured result. Our previous modeling of LEIS/DRS results for the W+H system appear to indicate that this is relatively constant<sup>30</sup>, so the contribution from this effect would be expected to only subtly change the result.

#### 4.2. p-T diagrams of the hydrogen coverage of the W(110) and W(100) surfaces

The resulting model provides a full quantitative agreement on W(110) and an overall quantitative agreement on W(100) for three experimental pressures investigated. It can be used as a predictive tool to determine the macroscopic coverage  $\bar{\theta}$  for any pressure  $p$  and temperature  $T$  in the range of validity of the model. To this end, **Figure 8** provides two dimensional  $p$ - $T$  diagrams of  $\bar{\theta}$  of both the W(110) and W(100) surfaces. As a general trend, saturation is obtained at low temperature and high pressure. On the other hand, high temperature and low pressure are energetically more favorable to the gas phase, leading to depletion of the surface

up to  $\theta = 0$ . More interestingly, both diagrams display very similar behavior: full, half and no coverage are met for very similar couples of  $p$ ,  $T$  coordinates.

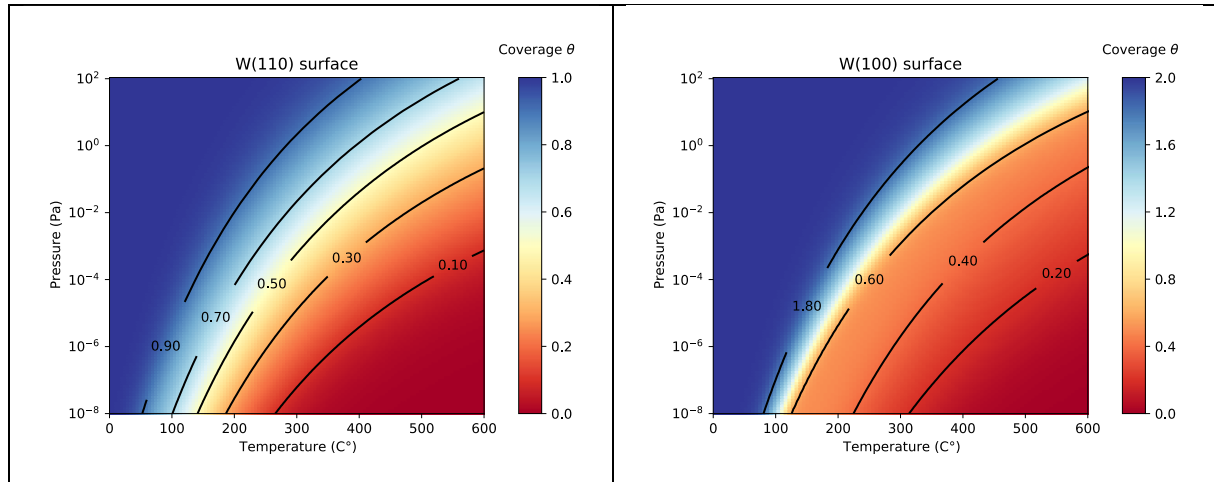


**Figure 8.** two-dimensional  $p$ - $T$  diagram of the macroscopic coverage  $\bar{\theta}$  for both the W(110) (*left plot*) and W(100) (*right plot*) surfaces. The thermodynamic model including the Gibb's free energy of a 1D gas was considered.

#### 4.3. Adsorption, desorption and recombination of H<sub>2</sub> on W(110) and W(100)

Adsorption, desorption and recombination of hydrogen on tungsten are processes that depend on the coverage of the surface as investigated herein. It was experimentally shown that the activation energy for the desorption of hydrogen from the W(100) surface significantly decreases from 1.6eV to 0.9eV when the coverage falls below  $\theta \approx 0.25 - 0.50$ <sup>36,37</sup>. The same trend was found on the W(110) surface<sup>38</sup>. These findings were recently confirmed by DFT calculations: Ajmalghan et al.<sup>17</sup> predicted a drop in desorption energy from 1.5eV at saturation in hydrogen to 0.8 eV below on both the W(110) and W(100) surfaces. The activation energy for recombination into molecular hydrogen was also shown to drop from 1.7 eV at saturation to 0.9eV below.

Thanks to the present model, the  $p$  and  $T$  dependence of the above results can now be revealed: in the blue regions of **Figure 8** where both surfaces are at saturation, the activation energies is



0.8eV for absorption of hydrogen and 0.9eV for recombination followed by desorption. In the red region of **Figure 8** where the surface is bare, the absorption energy is 1.5 eV and the recombination energy is 1.7eV. Such results can help establish a kinetic model of the surface, similar to the one recently developed by Hodille et al.<sup>11</sup>.

#### **4.4. Beyond the present thermodynamic model**

The present thermodynamic based DFT model reproduces well the low temperature configurations observed for hydrogen on W(110) and W(100) surfaces. It also very efficiently reproduces the experimental hydrogen coverage versus temperature for three different pressure. On the W(110) surface, the agreement with the experimental data is satisfactory despite the model is built based on a small number of DFT based configurations. A possible way to extend the model is to use the 31 configurations we computed on the W(100) and the 17 configurations on the W(110) surface to develop a model Hamiltonian for representing the energy of the system. This could be done thanks to a two-dimensional cluster expansion<sup>39,40</sup> of the DFT-computed adsorption energies, where the cut-off radius and the order of the cluster would be determined using the cross-validation score process. This would allow a methodical examination of a wider range of coverages and configurations on a larger working-cell. This also would enable us to check which relevant configuration is missing, if any, in order to build the partition function of the present thermodynamic model. However, the main issue to be solved is how to obtain the vibrational frequencies of the various configurations in a larger unit-cell. Indeed, adsorption energies depend on the temperature through the vibrational frequencies. This dependence is critical for reproducing isobaric coverage versus temperature trends. Since it is not computationally feasible to compute them by DFT, we will have to find a way to determine them by other means. This work will be considered by us in the near future.

## 5. CONCLUSION

We herein provided a thermodynamic model based on DFT data for the adsorption of hydrogen on W(110) and W(100). The results of the model were compared with LEIS and DRS experimental results. The general agreement is good between both set of data. Nevertheless, the model lacks a degree of freedom that takes into account the temperature-induced motion of the adsorbate on the surface. As the adsorbate is supposed to move along 1D channels on top of the corrugated potential energy surface of W(110) and W(100), we added to the model the Gibb's free energy of a 1D gas. The agreement is fully quantitative for W(110) and overall quantitative for W(100) due to the reconstruction of the surface. Finally, we discuss a possible pathway toward extending the size of the unit-cell, as well as the number of coverages and configurations considered in the partition function of the model. This could potentially open new avenues of future work.

### ■ SUPPORTING INFORMATION AVAILABLE

A schematic representation with their energetics for all computed configurations and coverages investigated is made available in the supporting information on the W(110) and W(100).

### ■ ACKNOWLEDGEMENTS

This work has been carried out within the framework of the French Federation for Magnetic Fusion Studies (FR-FCM) and of the Eurofusion consortium, and has received funding from the Euratom research and training program 2014–2018 and 2019–2020 under grant agreement No 633053. This work was performed under EUROfusion WP PFC. This work also received fund within the framework of the A\*MIDEX project (Grant No. ANR-11-IDEX-0001–02) funded by the Investissements d'Avenir French Government program, managed by the French

National Research agency. The views and opinions expressed herein do not necessarily reflect those of the European Commission. The authors of this paper were granted access to the high-performance computing resources of IDRIS and CINES under Allocation No. A0060806612 made by Grand Equipement National de Calcul Intensif and to the Marconi Supercomputer at CINECA Super Computing Application and Innovation Department, Bologna, Italy. RDK acknowledges support from the U.S. Department of Energy, Office of Fusion Energy Sciences, through the Materials Research Program. Sandia National Laboratories is a multimission laboratory managed and operated by National Technology and Engineering Solutions of Sandia LLC, a wholly owned subsidiary of Honeywell International Inc. for the U.S. Department of Energy's National Nuclear Security Administration under contract DE-NA0003525.

## ■ APPENDIX

The vibrational enthalpies and entropies were calculated as follows:

$$h_{vib} = \sum_{j=1}^{n_{vib}} h\nu_j \left( \frac{1}{2} + \frac{1}{\exp\left(\frac{h\nu_j}{k_B T}\right) - 1} \right) \quad (\text{A-1})$$

$$s_{vib} = k_B \sum_{j=1}^{n_{vib}} \left[ \frac{h\nu_j}{k_B T} \frac{1}{\exp\left(\frac{h\nu_j}{k_B T}\right) - 1} - \ln \left( 1 - \exp\left(-\frac{h\nu_j}{k_B T}\right) \right) \right] \quad (\text{A-2})$$

The translational and rotational components to the Gibbs free energy also have to be considered for the gas phase. Assuming H<sub>2</sub> behaves as an ideal homonuclear diatomic gas in the range of pressure here considered, the enthalpy and entropy components are calculated as follows:

$$h_{trans,H_2} = \frac{5}{2} k_B T \quad s_{trans}^{\circ} = k_B \left( \frac{5}{2} + \ln \left[ \frac{k_B T}{p^{\circ}} \left( \frac{2 \pi m k_B T}{h^2} \right)^{\frac{3}{2}} \right] \right) \quad (\text{A-3})$$

$$h_{rot,H_2} = k_B T \quad s_{rot} = k_B \left( 1 + \ln \left[ \frac{8 \pi^2 I k_B T}{\sigma h^2} \right] \right) \quad (\text{A-4})$$

In the above expressions,  $k_B$  and  $h$  are the Boltzmann and Planck constant,  $m$  the mass of molecular hydrogen,  $I$  its inertia momentum,  $\sigma = 2$  for homonuclear diatomic molecules, and  $p^{\circ}$  is the standard pressure of 1 bar.

Finally,

$$g_{H_2}(T, P) = h_{H_2}(T) - T \cdot s_{H_2}(T, p) \quad (\text{A-5})$$

$$\mu(T, P) = \frac{1}{2} g_{H_2}(T) = \mu^{\circ}(T) + RT \ln \left( \frac{p}{p^{\circ}} \right) \quad (\text{A-6})$$

## ■ REFERENCES

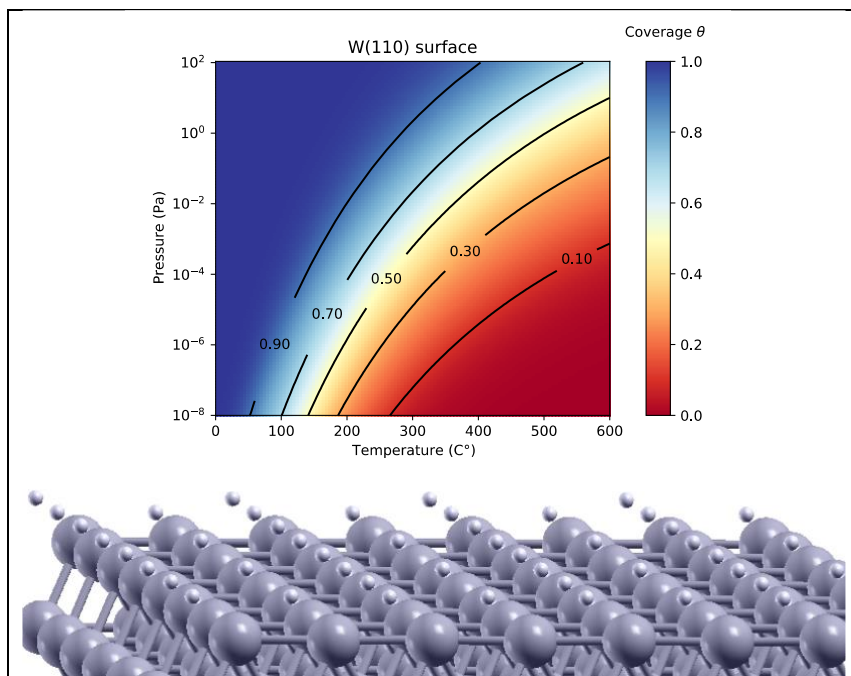
- (1) Kramers, H. A.; Wannier, G. H. Statistics of the Two-Dimensional Ferromagnet. Part I. *Phys. Rev.* **1941**, *60*, 252-262.
- (2) Onsagers, L. 117 Crystal Statistics. I.A Two-Dimensional Model with an Order-Disorder Transition. *Phys. Rev.* **1944**, *65*, 117-149.
- (3) Kreuzer H. J.; Payne S. H. In *Theoretical Approaches to the Kinetics of Adsorption, Desorption, and Reactions at Surfaces, In Equilibria and Dynamics of Gas Adsorption on Heterogeneous Solid Surfaces, Studies in Surface Science and Catalysis* Rudzifiski, W.; Steele, W.A.; Zgrablich, G., Eds., Elsevier Science B.V., 1997; Vol. 104 pp 153-200.
- (4) Ree, F. H.; Chesnut, D. A. Phase Transition of a HardCore Lattice Gas. The Square Lattice with Nearest Neighbor Exclusion, *J. Chem. Phys* **1966**, *45*, 3983-4003.
- (5) Payne S. H.; Zhang, J.; Kreuzer H. J. Lattice gas with multiple interactions: isosteric heat and thermal desorption, *Surface Science* **1992**, *264*, 185-196
- (6) Rikvold, P. A. ; Kaski, K.; Gunton, J. D.; Yalabik, M. C. Finite-size scaling study of a lattice-gas model for oxygen chemisorbed on tungsten, *Phys. Rev. B* **1984**, *29*, 62856294.

- (7) Matthews G.F. et al. (EFDA-JET Contributors), JET ITER-like wall—overview and experimental program, *Phys. Scr.* **2011**, 2011, 014001.
- (8) Philipps V.; Mertens P.; Matthews G.F. and Maier H. Overview of the JET ITER-like wall project, *Fusion Eng. Des.* **2020**, 85, 1581–6
- (9) Bucalossi J. et al. The WEST project: Testing ITER divertor high heat flux component technology in a steady state tokamak environment, *Fusion Eng. Des.* **2014** 89, 907–12.
- (10) Brezinsek S. et al. Plasma–wall interaction studies within the EUROfusion consortium: progress on plasma-facing components development and qualification, *Nucl. Fusion* **2017**, 57 116041.
- (11) Hodille E.A.; Markelj S.; Pecovnik M.; Piazza Z. A.; Ajmalghan M.; Ferro Y.; Schwarz-Selinger T.; Grisolia C. Kinetic model for hydrogen adsorption in tungsten with coverage dependent surface mechanism, *Nucl. Fusion* **2020**, 60, 106011.
- (12) Hodille E.A.; Založnik A.; Markelj S.; Schwarz-Selinger T.; Becquart C.S.; Bisson R.; Grisolia C. Simulations of atomic deuterium exposure in self-damaged tungsten, *Nucl. Fusion* **2017**, 57, 056002.
- (13) Založnik A.; Markelj S.; Schwarz-Selinger T.; Schmid K. Deuterium atom loading of self-damaged tungsten at different sample temperatures, *J. Nucl. Mater.* **2017**, 496, 1–8.
- (14) Matveev D.; Wensing M.; Ferry L.; Virost F.; Barrachin M.; Ferro Y.; Linsmeier Ch. Reaction-diffusion modeling of hydrogen transport and surface effects in application to single-crystalline Be, *Nucl. Instrum. Methods Phys. Res.* **2018**, B 430, 23–30.
- (15) Matveev D.; Hansen P.; Dittmar T.; Koslowski H. R; Linsmeier Ch. Modeling of H/D isotope-exchange in crystalline beryllium, *Nuclear Materials and Energy* **2019**, 20, 100682.
- (16) Guterl J.; Smirnov R.D.; Snyder P. Effects of surface processes on hydrogen outgassing from metal in desorption experiments, *Nucl. Fusion*, **2019**, 59, 096042.
- (17) Ajmalghan M.; Piazza Z. A.; Hodille E. A.; Ferro Y. Surface coverage dependent mechanisms for the absorption and desorption of hydrogen from the W(110) and W(100) surfaces: a DFT investigation, *Nuclear Fusion*, **2019**, 59, 106022.
- (18) Piazza Z. A.; Ajmalghan M.; Kolasinski R. D.; Ferro Y., A thermodynamic model of Hydrogen Coverage on the W(110) surface based on density functional theory, *Physica Scripta* **2020**, 2020, 014025.
- (19) Giannozzi P. et al., QUANTUM ESPRESSO: a modular and open-source software project for quantum simulations of materials, *J. Phys.: Condens. Matter*, 2009, 21, 395502.
- (20) Perdew J. P.; Burke K.; Ernzerhof M. Generalized gradient approximation made simple, *Phys. Rev. Lett.* **1996**, 77, 3865.
- (21) Vanderbilt D. Soft self-consistent pseudopotentials in a generalized eigenvalue formalism, *Phys. Rev. B*, **1990**, 41, 7892.

- (22) Baroni S.; de Gironcoli S.; Dal Corso A. Phonons and related crystal properties from density functional perturbation theory, *Rev. Mod. Phys.*, **2001**, *73*, 515.
- (23) Piazza Z. A.; Ajmalghan M.; Ferro Y.; Kolasinski R. D. Saturation of tungsten surfaces with hydrogen: a density functional theory study complemented by low energy ion scattering and direct recoil spectroscopy data, *Acta Materialia*, **2018**, *145*, 388-398.
- (24) Nojima A.; Yamashita K. A theoretical study of hydrogen adsorption and diffusion on a W(110) surface, *Surf. Sci.*, **2007**, *601*, 3003-3011.
- (25) Gonchar V.V.; Kanash O.V.; Naumovets A.G.; Fedorus A.G. Two-dimensional lattices of adsorbed hydrogen on the (011) face of tungsten and their disordering, *JETP Lett.*, **1979**, *28*, 330-333.
- (26) Balden M.; Lehwald S.; Ibach H. Substrate and hydrogen phonons of the ordered  $p(2 \times 1)$  and  $(2 \times 2)$  phase and of the anomalous  $(1 \times 1)$  phase of hydrogen on W(110), *Phys. Rev. B*, **1996**, *53*, 7479,
- (27) Barker R.A.; Estrup P.J. Hydrogen on Tungsten(100): adsorbate-induced surface reconstruction, *Phys. Rev. Lett.* **1978**, *41*, 1307-1310.
- (28) Kolasinski R.D.; Hammond K.D.; Whaley J.A.; Buchenauer D.A.; Wirth B.D. Analysis of hydrogen adsorption and surface binding configuration on tungsten using direct recoil spectrometry, *Journal of Nuclear Materials*, **2015**, *463*, 1053-1056.
- (29) Kolasinski R.D.; Bartelt N.C.; Whaley J.A.; Felter T. E. Channeling of low-energy ions on hydrogen-covered single-crystal surfaces, *Phys. Rev. B*, **2012**, *85*, 115422.
- (30) Heinola K.; Ahlgren T. Diffusion of hydrogen in bcc tungsten studied with first principle calculations, *J. Appl. Phys.*, **2010**, *107*, 113531.
- (31) Tamm P.W.; Schmidt L. D. Bonding states of hydrogen on tungsten, *J. Chem. Phys.*, **1971**, *54*, 4775.
- (32) Budi A.; Stipp S. L. S. Andersson M. P., Calculation of entropy of adsorption for Small molecules on mineral Surfaces, *J. Phys. Chem. C*, **2018**, *122*, 8236-8243.
- (33) Campbell C. T.; Sellers J. R. V. The entropies of adsorbed molecules, *J. Am. Chem. Soc.*, **2012**, *134*, 18109-18115.
- (34) Balden M.; Lehwald S.; Ibach H.; Mills D.L. Hydrogen covered W(110) surface: a hydrogen liquid with a propensity for one-dimensional order, *Phys. Rev. Lett.*, **1994**, *73* (1994), 854.
- (35) Bergstrom Z. J.; Li C.; Samolyuk G. D.; Uberuaga B. P.; Wirth B. D. Hydrogen interactions with low-index surface orientations of tungsten, *J. Phys.: Condens. Matter*, **2019**, *31*, 255002.
- (36) Alnot P.; Cassuto A.; King, D. A. Adsorption and desorption kinetics with no precursor trapping: hydrogen and deuterium on W(100), *Surf. Sci.*, **1989**, *215*, 29-46.

- (37) Horlacher Smith A.; Barker R.A; Estrup P.J., Desorption of hydrogen from tungsten (100), *Surf. Sci*, **1984**, *136*, 327-344.
- (38) Nahm T. U.; Gomer R., The adsorption of hydrogen on W(110) and Fe covered W(110) surfaces, *Surf. Sci*, **1997**, *375*, 281-292.
- (39) Samin A.J.; Taylor C. T.; A first principle investigation of the oxygen adsorption on Zr(0001) surface using cluster expansions. *Applied Surface Sciences* **2017**, *423*, 1035-1044.
- (40) Sluiter M. H. F., Kawazoe Y.; Cluster expansion method for adsorption: Application to hydrogen chemisorption on graphene, *Physical Review B* 2003, *68*, 085410.

■ TOC GRAPHIC





## ■ STATEMENTS

Conflict of interest: None

Author's contribution:

- Zachary A. Piazza: DFT calculations, contribution to writing the python thermodynamic model.
- Robert D. Kolasinski: did all experimental work with low energy ion beam analysis, wrote the experimental part of the paper
- Ajmalghan Muthali: DFT calculations
- Etienne A. Hodille: help in developing the thermodynamic model, wrote part of the paper (Introduction, discussion).
- Yves Ferro: PI, developed the Thermodynamic model, did the rest of writing the paper.

# A Predictive Atomistic Model for Hydrogen Adsorption on Metal Surfaces: Comparison with Low Energy Ion Beam Analysis on Tungsten

Z. A. Piazza<sup>a</sup>, R. D. Kolasinski<sup>b</sup>, M. Ajmalghan<sup>a</sup>, E. A. Hodille<sup>a</sup> and Y. Ferro<sup>a,\*</sup>

<sup>a</sup> *Laboratoire PIIM, Aix-Marseille Université/CNRS, Avenue escadrille Normandie-Niemen, 13397, Marseille, France*

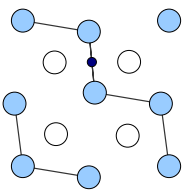
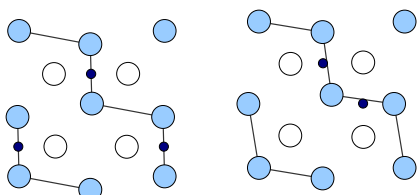
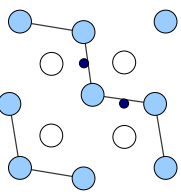
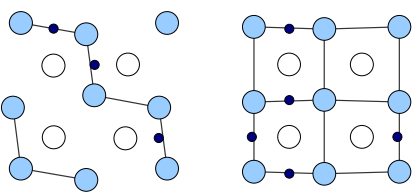
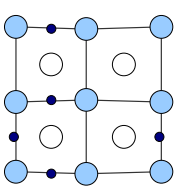
<sup>b</sup> *Sandia National Laboratories, Plasma and Reacting Flow Science Department, Livermore, California 94 551, USA*

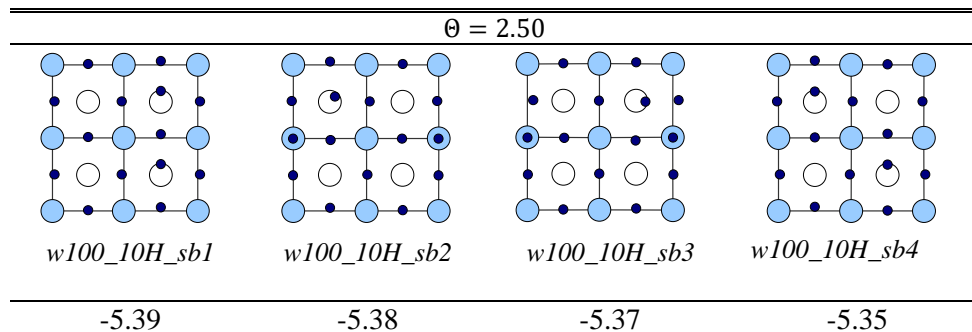
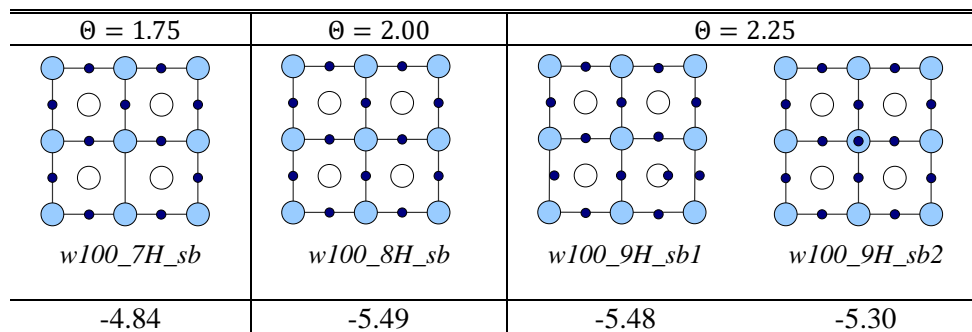
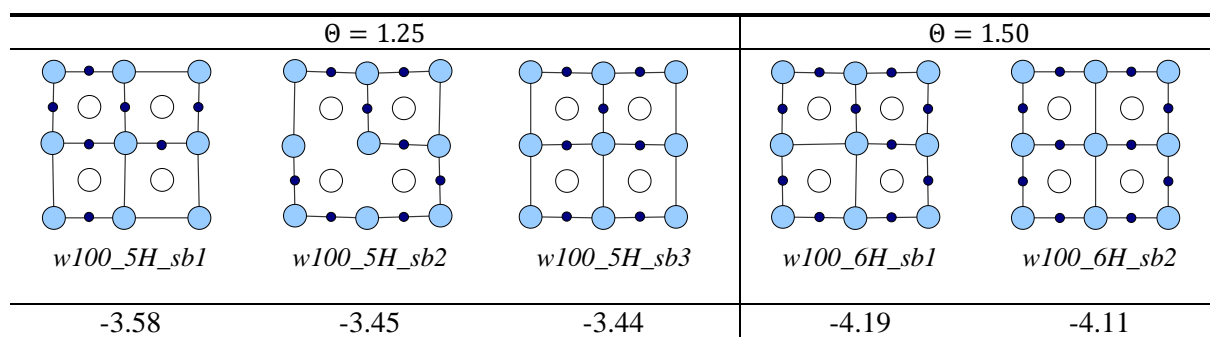
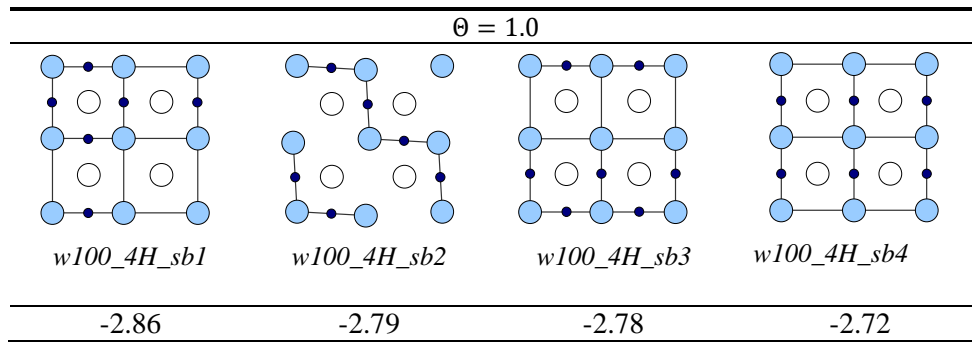
## Supplementary information

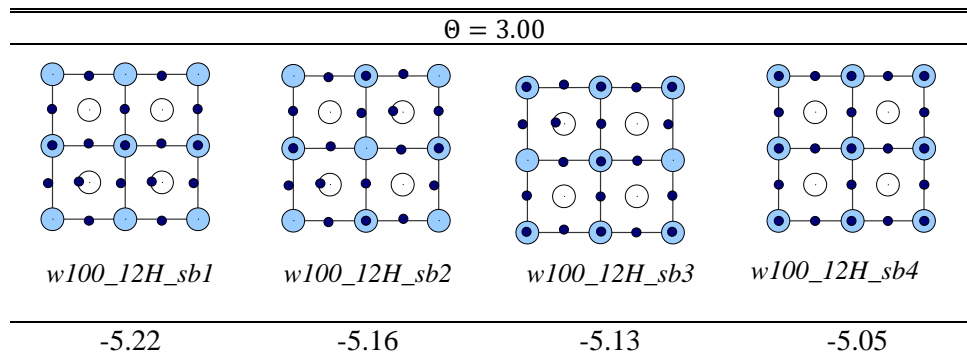
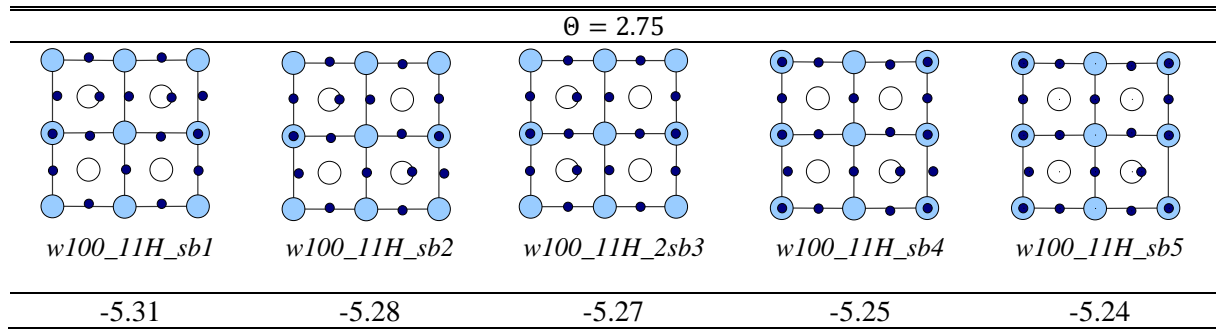
The values presented in the table below were calculated using the PBE exchange and correlation functional with the corresponding Vanderbilt USPPs for W and H, 260 bands (10 bands/W atom), and energy cutoffs of 40 Ry and 320 Ry for the wave-function and electron density, respectively. A k-point sampling of  $11 \times 11 \times 1$  for W (110) and  $9 \times 9 \times 1$  for W(100) were shown to be converged. Total electronic energy was considered self-consistent at a threshold of  $1.0 \times 10^{-7}$  Ry. Atomic coordinates were optimized to a force threshold of  $1 \times 10^{-5}$  eV/Å; subsequently phonons were calculated using DFT-PT holding all W atoms fixed in space until the forces were self-consistent to a threshold of  $1.4 \times 10^{-10}$  eV/Å.

In the tables, data are displayed as follows: the first line provides the hydrogen coverage, the second presents a cartoon of the geometry of adsorption, while the last line gives the adsorption energy corrected from the zero-point energy.

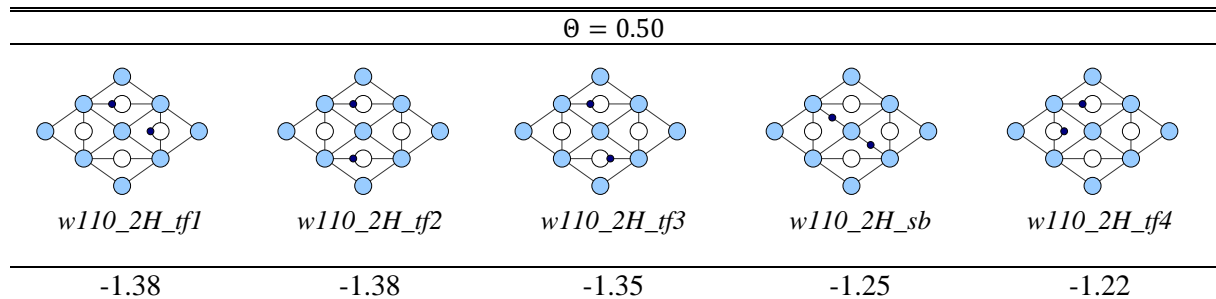
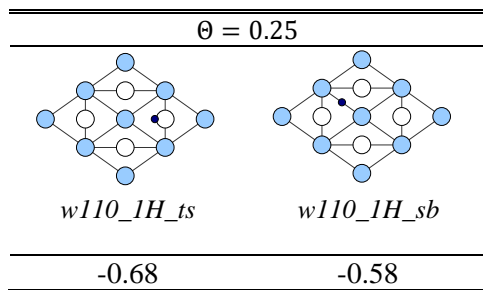
### 1 . W(100) Coverage specific data tables

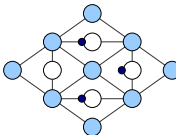
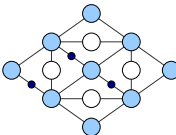
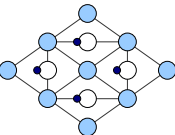
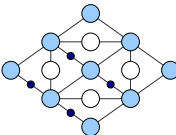
$\theta = 0.25$	$\theta = 0.50$		$\theta = 0.75$	
				
<i>w100_1H_sb</i>	<i>w100_2H_sb1</i>	<i>w100_2H_sb2</i>	<i>w100_3H_sb1</i>	<i>w100_3H_sb2</i>
-0.83	-1.69	-1.54	-2.22	-2.02

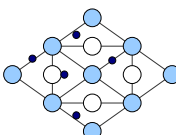
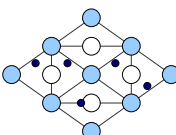
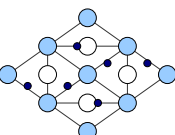
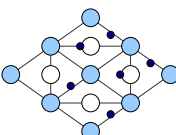


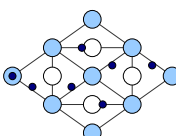
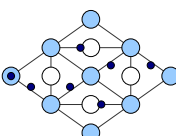


## 2. W(110) Coverage specific data tables



$\theta = 0.75$		$\theta = 1.00$	
			
<i>w110_3H_tf</i>	<i>w110_3H_sb</i>	<i>w110_4H_tf</i>	<i>w110_4H_sb</i>
-2.03	-1.75	-2.63	-2.24

$\theta = 1.25$		$\theta = 1.50$	
			
<i>w110_5H_tfsb1</i>	<i>w110_5H_tfsb1</i>	<i>w110_6H_tfsb1</i>	<i>w110_6H_tfsb2</i>
-2.62	-2.59	-2.69	-2.65

$\theta = 1.75$	
	
<i>w110_7H_1</i>	<i>w110_7H_2</i>
-2.44	-2.35